iScience, Volume *23*

Supplemental Information

SARS-CoV-2 Receptors and Entry Genes Are Expressed in the Human Olfactory Neuroepithelium and Brain

Leon Fodoulian, Joël Tuberosa, Daniel Rossier, Madlaina Boillat, Chenda Kan, Véronique Pauli, Kristof Egervari, Johannes A. Lobrinus, Basile N. Landis, Alan Carleton, and Ivan Rodriguez

Supplementary Figures

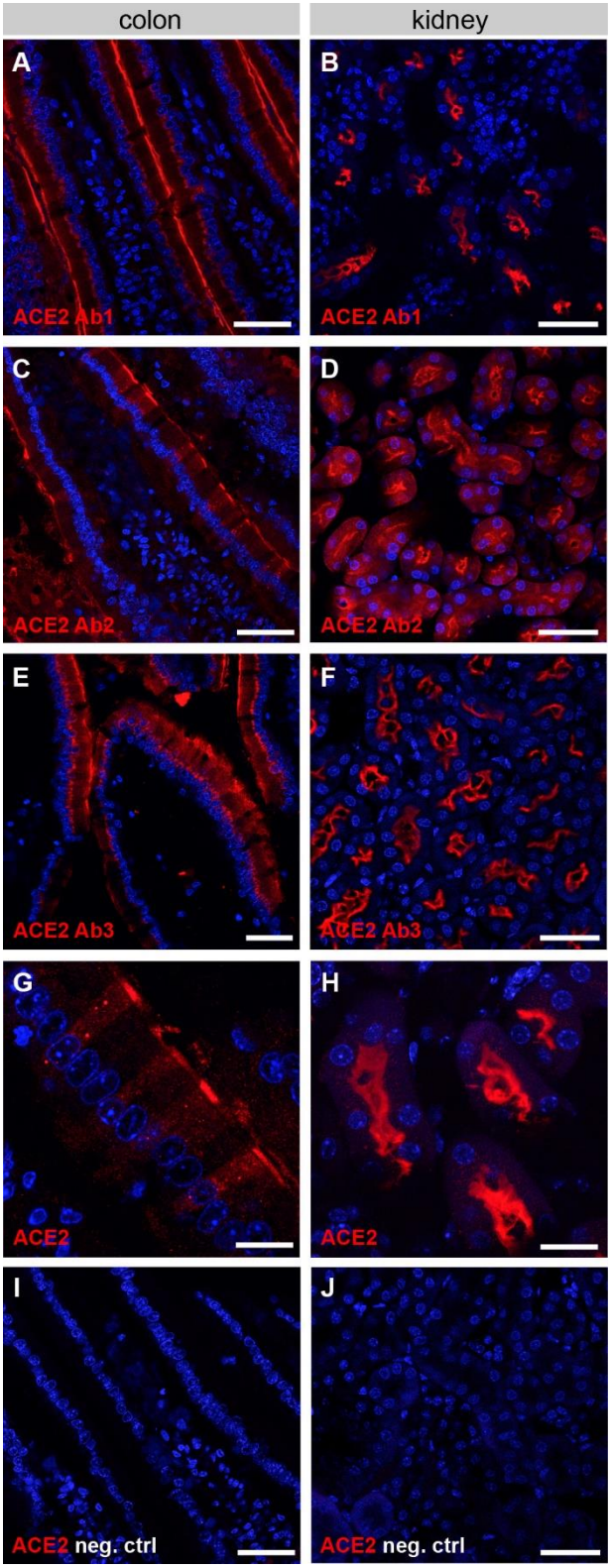

Figure S1. ACE2 expression in the mouse kidney and colon (related to Figure 3). (**A-H**) Evaluation of the three different anti-ACE2 antibodies. Immunostaining for ACE2 (red) on sections of mouse colon (left

panels) and kidney (right panels). (**A,B**) ACE2 Ab1, polyclonal antibody against the extracellular domain of mouse ACE2. (**C,D**) ACE2 Ab2, polyclonal antibody against the intracellular domain of human ACE2. (**E**,**F**) ACE2 Ab3, monoclonal antibody against the extracellular domain of human ACE2. Counterstaining with DAPI (blue). Scale bar: 40 µm. (**G,H**) Higher magnification of mouse colon (**G**) and kidney (**H**) sections immunostained for ACE2 (red). Scale bar: 20 µm. (**I,J**) Negative control immunostainings on colon and kidney without primary antibody for ACE2. Scale bar: 40 µm.

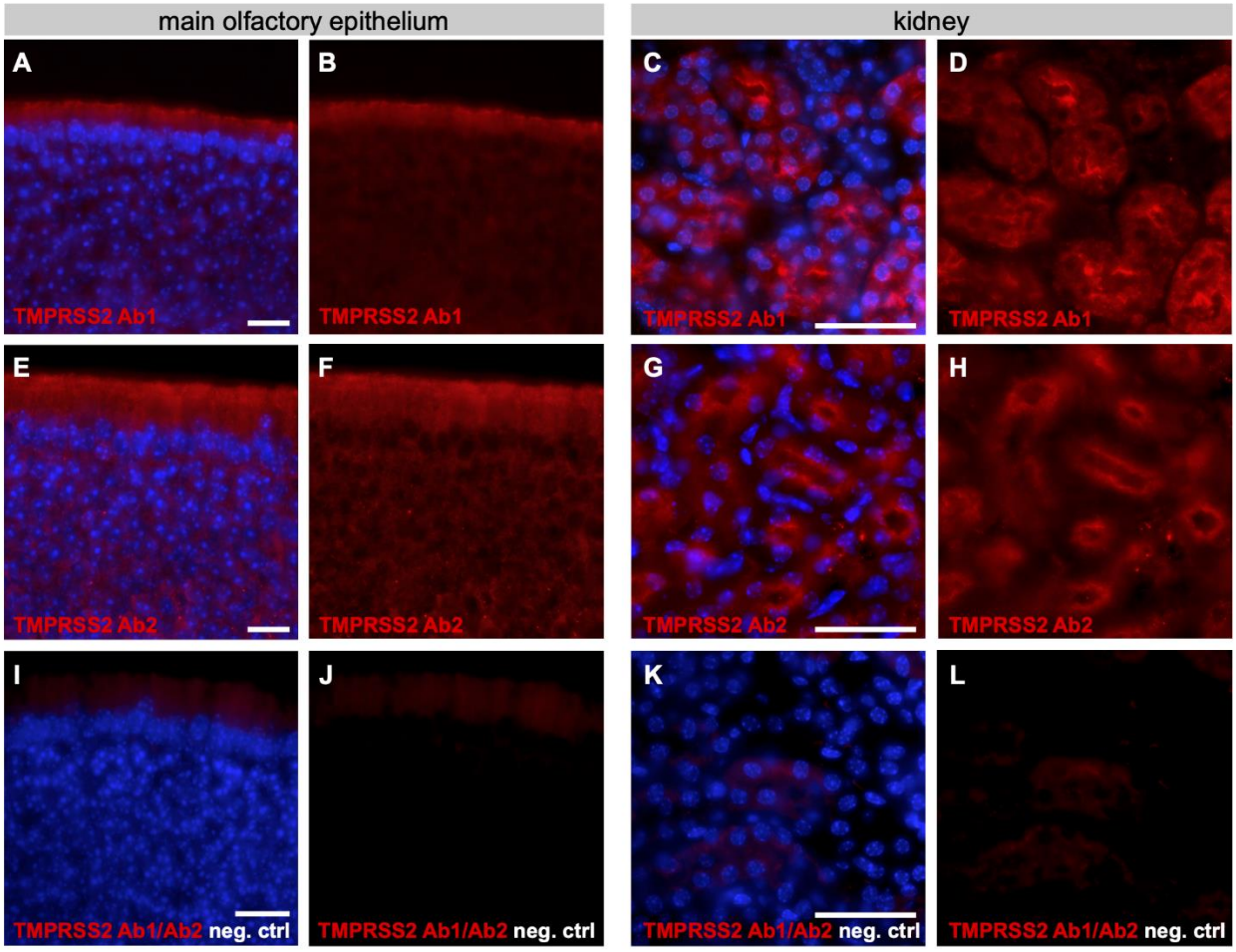

Figure S2. TMPRSS2 expression in the mouse olfactory epithelium and kidney (related to Figure 3). (**A-H**) Evaluation of the two different anti-ACE2 antibodies. Immunostaining for ACE2 (red) on sections of mouse olfactory epithelium (left panels) and kidney (right panels). For each staining, the same image is shown with and without DAPI staining (blue). (**A,B,C,D**) TMPRSS2 Ab1, monoclonal antibody against human TMPRSS2. (**E,F,G,H**) TMPRSS2 Ab2, monoclonal antibody against the C-terminus domain of human TMPRSS2. (**I,J,K,L**) Negative control immunostainings on main olfactory epithelium and kidney without primary antibody for TMPRSS2. Scale bars: 20 µm.

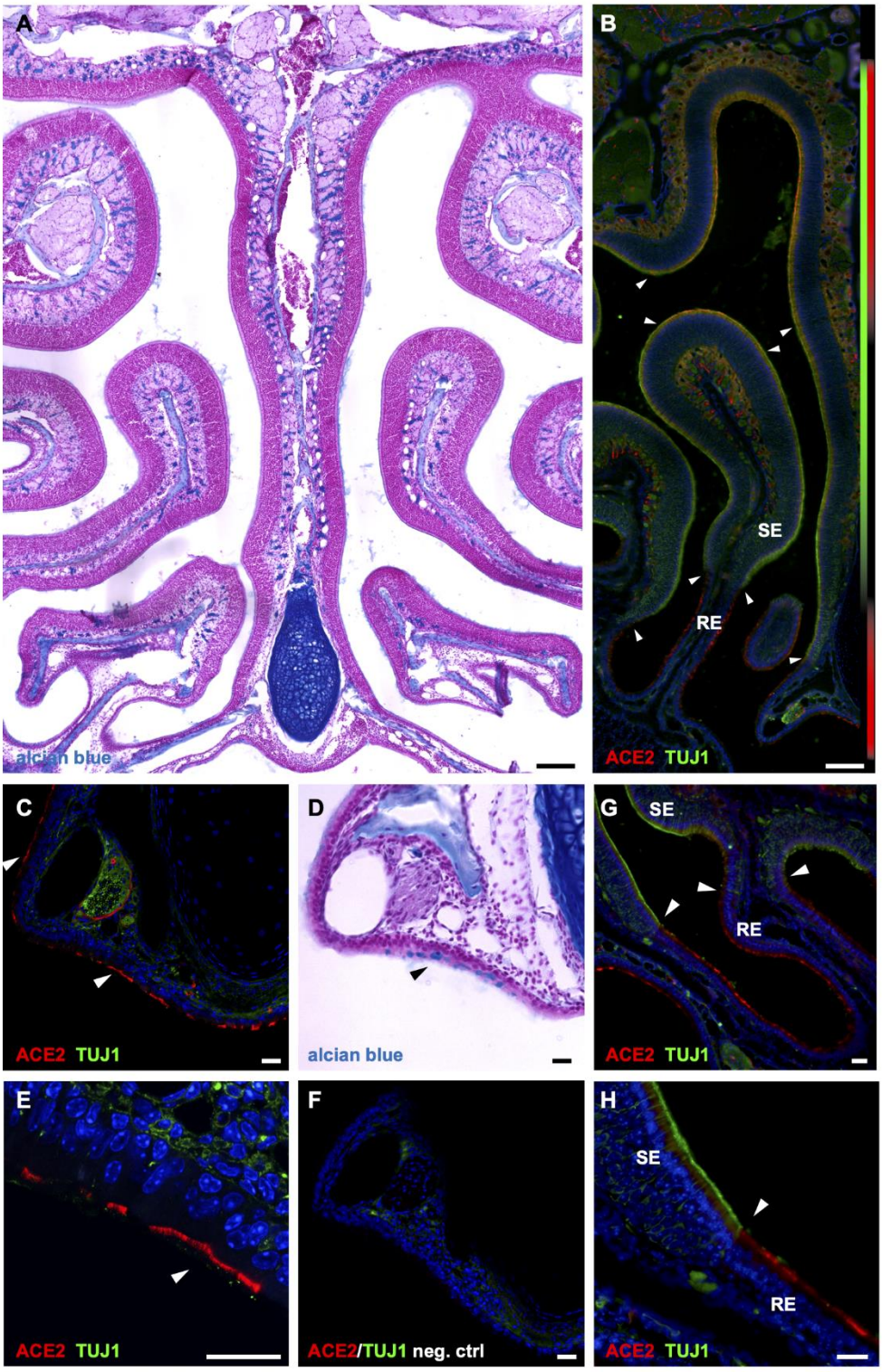

Figure S3. ACE2 expression in the mouse olfactory and respiratory epithelium (related to Figure 3). (**A**) Alcian blue staining on a coronal section of the mouse olfactory neuroepithelium. The entire sensory epithelium is devoid of goblet cells. Scale bar: 0.2 mm. (**B**) Immunostaining for ACE2 (red) and the neuronal marker TUJ1 (green) on a section of mouse nasal cavity and nasopharyngeal duct. White arrowheads indicate transitions from ACE2-positive to ACE2-negative zones. Colored bars on the right show expression

zones of ACE2 (red) and TUJ1 (green). ACE2 is expressed in the dorsal olfactory epithelium and in the ventral respiratory epithelium. SE: sensory epithelium, RE: respiratory epithelium. Scale bar: 0.2 mm. (**C-H**) Evaluation of ACE2 expression in the mouse respiratory epithelium. (**C,E**) Immunostaining for ACE2 (red) and the neuronal marker TUJ1 (green) on sections of respiratory epithelium in the nasopharyngeal duct. (**D**) The same section with alcian blue staining, showing the presence of goblet cells. (**F**) Negative control immunostaining without primary antibodies. (**G,H**) Immunostaining for ACE2 (red) and the neuronal marker TUJ1 (green) on the ventral part of the nasal cavity, showing the transition from olfactory to respiratory epithelium (white arrowhead). Scale bar: 40 µm. (**H**) Higher magnification of the transition zone shown in (**G**). When not indicated, scale bars are 20 µm. All sections with immunostaining were counterstained with DAPI (blue).

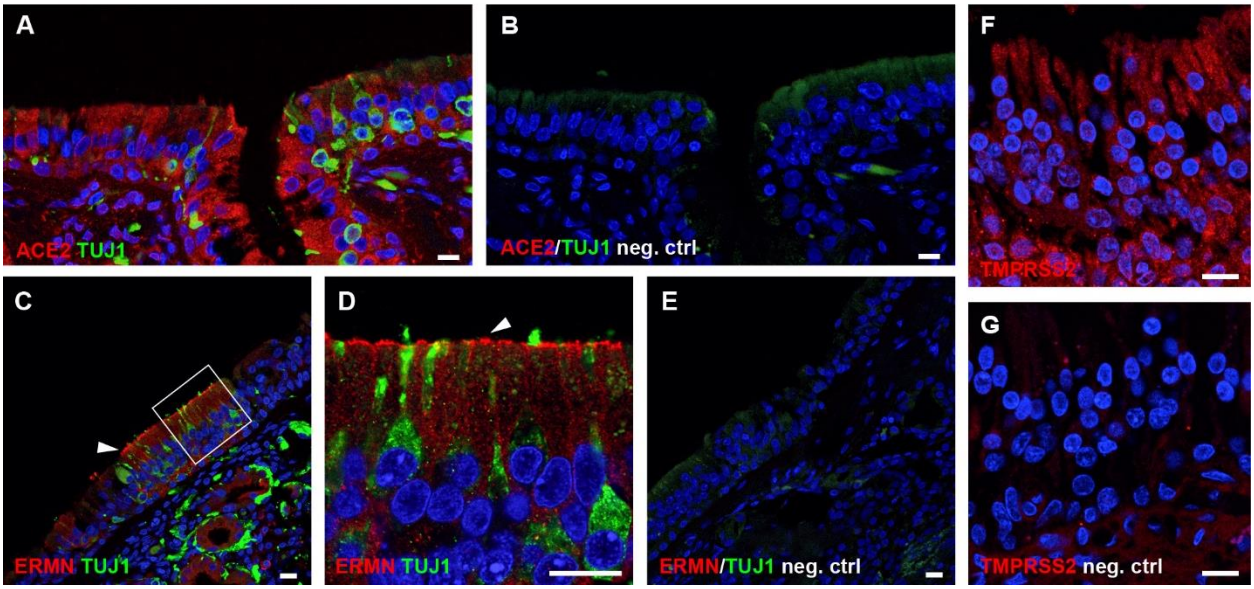

Figure S4. *ACE2* expression in the human olfactory neuroepithelium (related to Figure 4). (**A**) Section of human olfactory neuroepithelium immunostained for ACE2 (red) and for the neuronal marker TUJ1 (green). (**B**) Same region as in (**A**), immunostained without primary antibodies. (**C, D, E**) Section of human olfactory neuroepithelium immunostained for the sustentacular cell marker ERMN (red) and the neuronal marker TUJ1 (green). The white square in (**C**) highlights the region magnified in (**D**). ERMN is expressed in the apical portion of sustentacular cells (white arrowheads). (**E**) Same region as in (**D**), but without primary antibodies. (**F**) Section of human olfactory neuroepithelium immunostained for TMPRSS2 (red). (**G**) Same region as in (**F**), immunostained without primary antibody. All sections with immunostaining were counterstained with DAPI (blue). Scale bars: 10 µm.

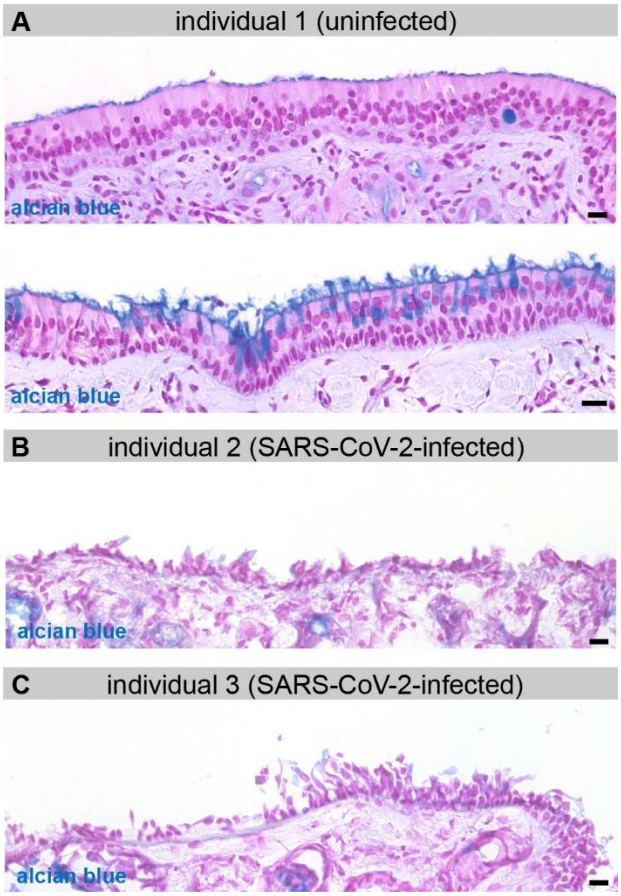

Figure S5. Damaged olfactory epithelium of deceased patients infected with SARS-CoV-2 (related to Figure 4). (**A**) Sections of uninfected human olfactory neuroepithelium (upper panel) and respiratory epithelium (lower panel) stained with alcian blue. (**B**) and (**C**) Sections of human olfactory neuroepithelium from patients infected by SARS-CoV-2 stained with alcian blue. Scale bars: 10 µm.

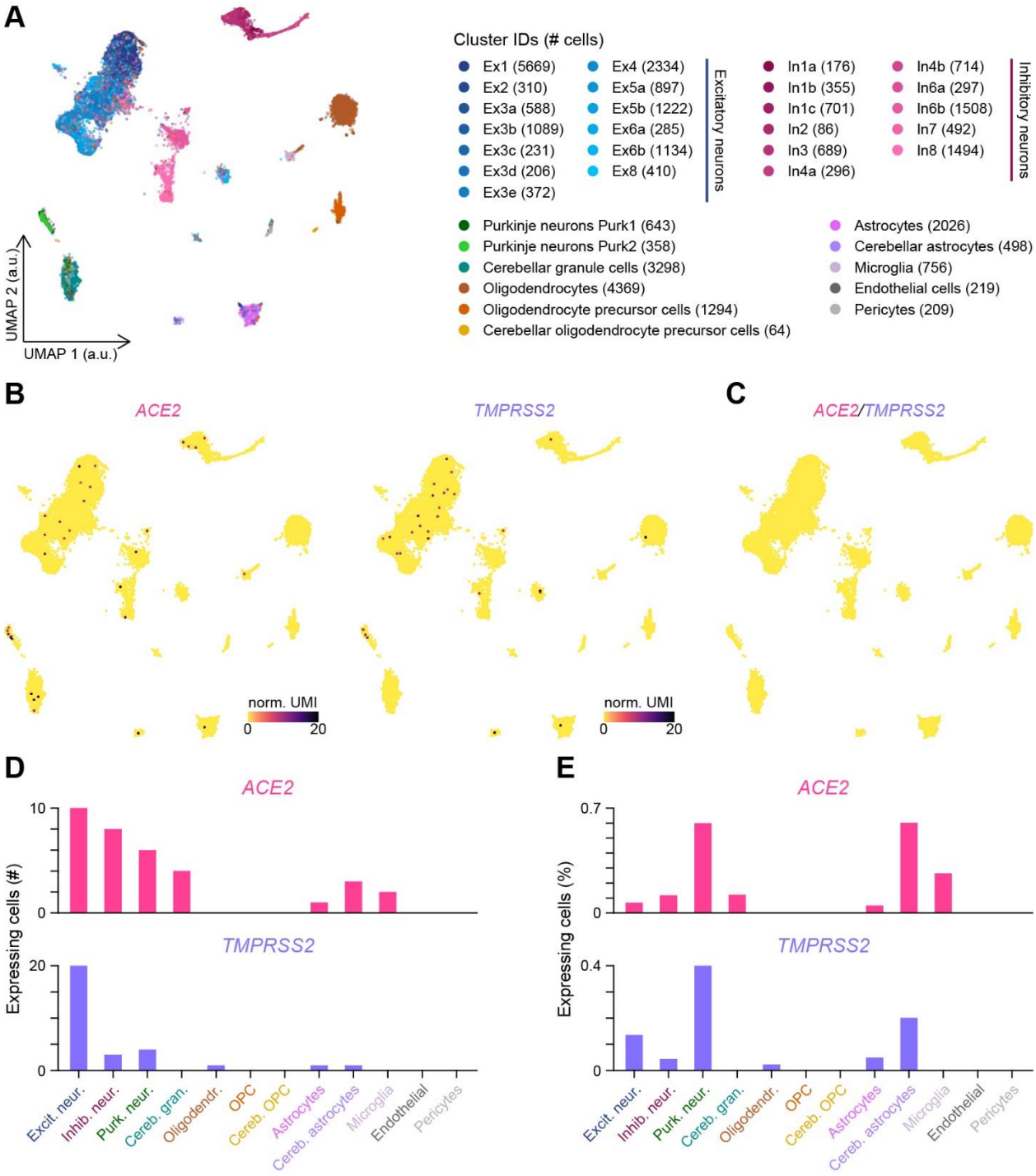

Figure S6. *ACE2* and *TMPRSS2* expression in the human brain (related to Figure 6). (**A**) Visualization of the clustering results reported in Lake et al.(Lake et al., 2018) on a UMAP plot. a.u.: arbitrary units. (**B**) Normalized expression levels of *ACE2* and *TMPRSS2* shown on the UMAP plot. Color gradient scales are in $\log_{10}$. norm. UMI: normalized unique molecular identifier counts. (**C**) Absence of *ACE2* and *TMPRSS2* coexpressing cells highlighted on the UMAP plot. (**D,E**) Number (**D**) and percentage (**E**) of cells per cluster expressing *ACE2* or *TMPRSS2*. Combined results are shown for clusters with subdivisions (excitatory, inhibitory or Purkinje neuron clusters).

Transparent Methods

Human biopsies and bulk RNA sequencing

After authorization from the University of Geneva ethics commission (authorization CE-13-115) and the informed consent from all subjects, human biopsies were collected at the Geneva University Hospital. For whole tissue RNA-seq, samples of 4 individuals (3 males and 1 females, age between 45-55 years) were resected during nasal cavity surgeries under general anesthesia. Biopsies consisted in small pieces of tissue of approximately 3 mm in diameter, from the respiratory or the sensory epithelia. Biopsies were snap frozen in liquid nitrogen immediately upon collection. One patient had only an OE biopsy and another only a RE biopsy. For RNA extraction, tissues were placed in RLT Buffer (Qiagen) with beta-mercaptoethanol and lysed with stainless steel balls (5mm diameter, Schieritz and Huenstein AG) using a homogenizer (Big Prep, MB Biomedicals). Total RNA was isolated using RNeasy Mini Kit (Qiagen) following the manufacturer protocol. The quality and quantity of total RNA were evaluated with a Bioanalyzer (Agilent). Stranded cDNA libraries with suitable adapters for multiplexing were generated with Truseq RNA and DNA sample preparation kits (Illumina) following ribodepletion of the total RNA (200ng of total RNA per sample). Samples were multiplexed for sequencing in a HiSeq®2500 Sequencing system, generating 100bp single-end reads. Each patient represented an independent biological replicate.

Bulk RNA sequencing data analysis

RNA-seq reads were mapped onto the GRCh38 human genome assembly with STAR (Dobin et al., 2013) version 2.7.0a using the Ensembl v99 gene annotation file (GTF). Mutlimapped reads were filtered out with the option --outFilterMultimapNmax set to 1. Reversely stranded gene expression quantification was carried using featureCounts (Liao et al., 2014) version 1.6.3 and a modified version of the aforementioned GTF file. The records corresponding to *AC097625.2*, a newly annotated long non-coding RNA that spans and shares most exons of *ACE2*, were removed from the GTF file as they hampered *ACE2* quantification (due to ambiguous read counting). This gene had a total

of 3 detected counts in two samples and its removal from the GTF file led on average to a 9-fold increase in *ACE2* counts. Note that this annotation was absent from and did not affect the single-cell RNA-sequencing datasets as it first appeared in the GENCODE release 30 and the Ensembl release 96 of the GRCh38 GTF files. Differential gene expression analysis between olfactory epithelial (OE) biopsies and respiratory epithelial (RE) biopsies was performed using the DESeq2 (Love et al., 2014) Bioconductor package version 1.22.2 in R version 3.5.0. After fitting a negative binomial generalized linear model (GLM), the Wald test (two-tailed) was used to test for significance of gene expression differences as a function of biopsies at a $\log_2$ fold change threshold of 0. To control the false discovery rate, the Wald test p-values were adjusted for multiple comparisons using the Benjamini–Hochberg procedure (Benjamini and Hochberg, 1995). Patient identifications were not added to the model to control for potential differences in gene expression between individuals (i.e. batch effects) due to the underpowered experimental design highlighted by the 3 samples per condition. The Approximate Posterior Estimation for GLM coefficients (an adaptive Bayesian shrinkage estimator) implemented in the apeglm (Zhu et al., 2019) Bioconductor package version 1.4.2 was used to shrink $\log_2$ fold changes. During shrinkage, the maximum likelihood estimates (i.e. $\log_2$ fold changes) and their associated standard errors (both in log scale) were used to adapt the scale of the prior. The results of this analysis are represented as a volcano plot in Figure 1C. To display the expression levels of selected genes in individual samples (Figure 1D-1G), TPM values were calculated for each gene within each sample to normalize for sequencing depth differences. Olfactory cascade genes (i.e. *OMP*, *CNGA2* and *ANO2*) and the top 4 most differentially expressed OR genes (with the lowest adjusted *p*-values) were selected as markers of the olfactory neurosensory epithelium. ERMN was selected as a marker of sustentacular cells (Liang, 2018; Tang et al., 2009).

Droplet-based single-cell RNA sequencing data analysis of human olfactory epithelial cells

Data download: The processed 10X Genomics output files of all four patients of the single-cell RNA-seq dataset reported in Durante et al. (Durante et al., 2020) were downloaded from NCBI GEO: GSE139522. This dataset consists in human olfactory and respiratory

epithelial cells collected from four patients aged between 41 and 52 years. The data was analyzed in R version 3.5.0 using the Seurat (Butler et al., 2018; Satija et al., 2015; Stuart et al., 2019) R package version 3.1.4 following the indications described in Durante et al. (Durante et al., 2020) and using custom scripts.

Cell and gene filtering: The 10X files were loaded into R using the Read10X function of Seurat. A single Seurat object for all four patients was created using the CreateSeuratObject function of Seurat. At this step, genes not expressed in at least 3 cells at a threshold of a minimum of 1 UMI count were excluded from the analysis (min.cells = 3). The percentage of mitochondrial counts was then calculated for each cell using the PercentageFeatureSet function of Seurat. Cells were removed from the analysis if they had less than 400 detected UMI counts, expressed less than 100 or more than 6000 genes, and if their mitochondrial counts exceeded 10% of their total counts. This filtering resulted in retaining 28,726 cells and 26,439 genes.

Dataset integration: The standard Seurat version 3 (Stuart et al., 2019) integration workflow was used to integrate the data from all patients, as described in Durante et al. (Durante et al., 2020) First, the data from each patient was separated using the SplitObject function of Seurat. The raw UMI counts of each gene within each cell were normalized by the total number of UMI counts per cell, scaled to 10^4 and natural-log-transformed after adding a pseudocount of 1 using the NormalizeData function of Seurat (normalization.method = "LogNormalize"; scale.factor = 10000). The top 5000 variable genes were then determined in each dataset using the variance-stabilizing transformation (Stuart et al., 2019) method of the FindVariableFeatures function of Seurat (selection.method = "vst"; nfeatures = 5000). To assemble all datasets, integration anchors (i.e. mutual nearest neighbors) across the four datasets were identified with the FindIntegrationAnchors function of Seurat after computing the first 30 dimensions of the canonical correlation analysis(Butler et al., 2018) between each pair of datasets using the top 5000 variable genes shared between most datasets (reduction = "cca"; dims = 1:30; anchor.features = 5000; l2.norm = TRUE). The IntegrateData function of Seurat was then used to integrate all four datasets into a single Seurat object.

UMAP plot generation: To generate a UMAP (Becht et al., 2018; McInnes et al., 2018) plot, the integrated data was scaled and centered using the ScaleData function of Seurat and the first 30 principle components were computed using the RunPCA function of Seurat. These 30 principle components were then used as input to the RunUMAP function of Seurat (dims = 1:30). The UMAP plot was generated with the uwot R package version 0.1.8 implementation. The cosine metric was used to measure distance and find the nearest neighbors (metric = "cosine"), the number of neighbors used for the approximation of the manifold structure was set to 30 (n.neighbors = 30) and the effective minimum distance between embedded points was set to 0.3 (spread = 1; min.dist = 0.3). The clusters identified by Durante et al.(Durante et al., 2020) were displayed on the UMAP plot (Figure 2B) and were used for subsequent analyses. The cluster corresponding to “Respiratory columnar cells” was renamed as “Respiratory early secretory cells” based on its expression of *SERPINB3* (see Supplementary Table 3 from Durante et al. (Durante et al., 2020)).

Gene expression analysis and plotting: All gene expression analyses were performed using the actual normalized UMI counts (not log-transformed) from the non-integrated assay of the Seurat object. However, the scales of the axes in the violin plots (Figure 2A, F and G) and the color gradient scales in the heatmap plots (Figure 2C) are in $\log_{10}$ after adding a pseudocount of 1 to the normalized UMI counts. The axes in Figure 2E, 2H and 2I are not in log scale. *ACE2* and *TMPRSS2* coexpressing cells were identified as expressing at least 1 UMI count of both genes (Figure 2D). All violins in each violin plot have the same maximum width.

Droplet-based single-nucleus RNA sequencing data analysis of human brain cells

Data download: The digital gene expression matrices of the single-nucleus Drop-seq dataset reported in Lake et al. (Lake et al., 2018) were downloaded from NCBI GEO: GSE97930. This dataset consists in human brain nuclei collected from the frontal cortex, visual cortex and lateral cerebellar hemisphere from six individuals aged between 20 and 49 years (for more information, see Supplementary Table 1 from Lake et al. (Lake et al., 2018)). The data was analyzed in R version 3.5.0 using the pagoda2 R package

(https://github.com/hms-dbmi/pagoda2) version 0.1.1 following the indications described in Lake et al. (Lake et al., 2018) and using custom scripts. For simplification, the word “cells” will be used instead of “nuclei” in the following paragraphs.

Cell and gene filtering: All cells from the downloaded matrices had a cell type annotation and were therefore retained for further analysis. Genes shared between all 3 datasets (i.e. frontal cortex, visual cortex and lateral cerebellar hemisphere) were selected for downstream analysis. The final UMI count matrix, after combining all datasets, contained 35,289 cells and 31,302 genes.

Batch correction and data preparation: A new Pagoda2 object was created and the library identification of each cell was defined for batch correction using the plain model (see Supplementary Table 2 from Lake et al. (Lake et al., 2018)). Winsorization was used to clip the expression levels of each gene at the eleventh most extreme value (i.e. winsorizing the ten most extreme values; trim = 10). Batch-corrected gene expression levels were then normalized by the total number of counts per cell, scaled to 10^3 and natural-log-transformed after adding a pseudocount of 1.

UMAP plot generation: The variance of genes were calculated and adjusted using the adjustVariance function of pagoda2, as described in Lake et al. (Lake et al., 2018) (the smoothing term of the generalized additive model was set to gam.k = 10). The 2,000 overdispersed genes were then selected from the variance adjusted matrix and the 150 principle components were computed using the calculatePcaReduction function of pagoda2 (n.odgenes = 2000; nPcs = 150). These 150 principle components were then used to generate a UMAP plot with the getEmbedding function of pagoda2 (type = "PCA"; embeddingType = "UMAP"). As for the analysis of human olfactory epithelial cells, the uwot R package version 0.1.8 implementation was used to generate the UMAP plot. Also, the cosine metric was used to measure distance and find the nearest neighbors (distance = "cosine"), the number of neighbors used for the approximation of the manifold structure was set to 15 (n_neighbors = 15) and the effective minimum distance between embedded points was set to 0.1 (spread = 1; min_dist = 0.1).

Gene expression analysis and plotting: To plot the expression levels of *ACE2* and *TMPRSS2* on the UMAP projection in the form of a heatmap, the raw UMI counts of each gene within each cell were normalized by the total number of UMI counts per cell and scaled to 10^4. Similar to Figure 2C, the color gradient scales in the heatmap plots (Supplementary Figure 6B) are in $\log_{10}$ after adding a pseudocount of 1 to the normalized UMI counts. In Supplementary Figure 6D and 6E, broader clusters were defined by separately grouping all excitatory neuron clusters, all inhibitory neuron clusters and all Purkinje neuron clusters.

SMART-Seq v4 single-nucleus RNA sequencing data analysis of human brain cells

Data download: The digital gene expression matrix (matrix.csv), the *t*-SNE coordinates for each cell (tsne.csv) and the metadata table corresponding to the cells (metadata.csv) were downloaded from the Allen Brain Map cell types database, available online at https://portal.brain-map.org/atlases-and-data/rnaseq/human-multiple-cortical-areas-smart-seq. This dataset consists in human brain nuclei collected from three individuals and from eight brain regions: middle temporal gyrus (MTG), cingulate gyrus (CgG), primary visual cortex (V1C), primary auditory cortex (A1C), upper limb (ul) and lower limb (lm) regions of both primary motor cortex (M1) and primary somatosensory cortex (S1) (for more information, see metadata.csv from the website above). The data was analyzed in R version 3.5.0 using custom scripts. Like in the above paragraphs, the word “cells” will be used instead of “nuclei” in the following paragraphs.

Cell and gene filtering: Cells lacking a brain cell-type subclass annotation (subclass_label column from metadata.csv) and a *t*-SNE embedding were removed from the analysis, and all genes were retained for data normalization. The final expression matrix contained 47,432 cells and 50,281 genes.

Gene expression analysis and plotting: Prior to any gene expression plotting or analysis, the raw counts of each gene within each cell were normalized by the total number of counts per cell and scaled to 10^4. Similar to Figure 2C, the color gradient scales in the heatmap plots (Figure 6B and 6C) are in $\log_{10}$ after adding a pseudocount of 1 to the

normalized counts. However, the axes in Figure 6E, F and G are not in log scale. Also, as described above, *ACE2* and *TMPRSS2* coexpressing cells were identified as expressing at least 1 raw count of both genes (Figure 6D).

Data visualization and programming tools

All plots in Figures 1, 2 and 6, as well as in Figure S6, were generated using ggplot2 version 3.3.0. Other R and Bioconductor packages used for data analysis and plotting include rtracklayer(Lawrence et al., 2009) version 1.46.0, Matrix version 1.2.18, reshape2 version 1.4.3, data.table version 1.12.8, dplyr version 0.8.5, stringr version 1.4.0, ggrepel version 0.9.0, lemon version 0.4.4, extrafont version 0.17, viridis version 0.5.1, RColorBrewer version 1.1.2, patchwork version 1.0.0 and grid version 3.5.0.

Mouse brain cell database mining

For mouse brain single-cell transcriptomes, the datasets of Zeisel et al. (Zeisel et al., 2018) (Figure 5A and 5B) and Sauders et al. (Saunders et al., 2018) (Figure 5C) were analyzed from their respective websites: http://mousebrain.org/ and http://dropviz.org/.

Immunohistochemistry and histology

Tissue fixation and preparation: All animal procedures were performed in accordance with the guidelines and regulations of the institution and of the state of Geneva. Mice (C57BL6, Charles River Laboratories, France) were deeply anesthetized with Pentobarbitalum natricum at 150mg/kg (Streuli Pharma) and perfused transcardially with 1x phosphate-buffered saline (PBS)-heparine 20'000 UI/l (Bichsel), pH 7.4. After flushing, mice were perfused with 10% neutral buffered Formalin. Tissues were extracted and fixed over night at 4°C and cryoprotected in 15% sucrose, 1x PBS over night at 4 °C followed by 30 % sucrose, 1x PBS over night at 4 °C. Tissues were embedded in optimal cutting temperature compound (OCT) (Carl Roth, ref. 6478.1) and cut on a cryostat in 16 µm sections that were mounted on Superfrost+ slides. Sections were conserved at -80°C until use. For human post-mortem samples a written consent for the anonymized research use of biological material was obtained from relatives, in accordance with the guidelines and

regulations of the institution and of the state of Geneva. Human olfactory and respiratory epithelia were sampled from autopsies (individual 1: female, 90 years, uninfected with SARS-CoV-2; individual 2: male, 54 years, infected with SARS-CoV-2, individual 3: male, 86 years, infected with SARS-CoV-2. By transcranial access, the cribriform plate with the superior part of the nasal cavities and the septum nasi were removed. The postero-lateral and postero-medial parts of the nasal mucosa were carefully dissected and fixed in 10% neutral buffered Formalin for 48 hours and bony particles were decalcified in EDTA for 24 hours. Paraffin embedding was done using a standard protocol using a LOGOS Microwave Hybrid Tissue Processor (Milestone). Paraffin blocks were cut at 3 µm thickness with a microtome and mounted on Superfrost slides. Before staining, cryosections were thawed and dried for 30 min under a ventilated hood. Sections were re-hydrated with 1x PBS for 5 min. Paraffin sections were deparaffinized by placing them for 10 min in xylene (Fluka), and then successively for 1 min each in ethanol 100%, 90%, 80%, 70% and H_2O.

Alcian blue staining: For alcian blue staining, hydrated sections were stained for 30 min in alcian blue (Sigma, ref. 1.01647), acetic acid 3%, pH 2.5. Sections were washed for 2 min in running tap water and rinsed in distilled water. Sections were counterstained with 0.1% nuclear fast red, 5% aluminum sulfate solution (Merck Millipore, ref. 1.00121) for 5 min. Sections were washed for 1 min in running tap water and dehydrated. Sections were cleared in xylene and mounted with Eukitt (Sigma, ref. 03989) mounting medium.

Immunohistochemistry: For antigen retrieval, sections were immersed in 10mM Citric Acid, 0.05% Tween 20, pH 6.0 buffer previously heated to 95-100 °C, and incubated for 20 min. Sections were then cooled down to room temperature in 1x PBS. Section were pre-incubated for 30 min with 1x PBS containing 0.5% Triton X-100 and 5% FCS. Sections were incubated with primary antibodies (see details in Table S1) diluted in 1x PBS containing 0.5% Triton X-100 and 5% FCS over night at 4°C. Sections were washed 3x15 min with 1x PBS containing 0.5% Triton X-100. Sections were incubated with secondary antibodies diluted 1:800 in 1x PBS with 0.5% Triton X-100 and 5% FCS for 90 min at room temperature (see details in Table S2). Sections were again washed 3x 15 min with 1x PBS containing 0.5% Triton X-100. Sections were counterstained with DAPI

(1:5000) for 5 min, rinsed with 1x PBS and mounted with DABCO (Sigma) in glycerol. For all tissue samples and all conditions, control samples were processed simultaneously without applying primary antibodies.

Microscope imaging: Confocal imaging was performed with a Leica TCS SP8 using a PMT detector for DAPI fluorescence and HyD 5 detectors for Alexa488, Alexa555 and Cy3 fluorescence. Epifluorescence imaging was performed with a Leica DM5500 equipped with a DFC9000 GT monochrome camera. For both fluorescence microscopy techniques, illumination and detection was manually adjusted to optimize signal-to-noise ratio and minimize over-exposure, bleaching and light scattering. Brightfield imaging was performed with a Leica DM5500 equipped with a DMC2900 camera. Microscope automated control and image encoding was performed with the LAS X software version 3.4.2. Acquisition settings were matched in negative controls.

Microscope image editing: Maximum intensity projection were computed on the LAS X software for z-stack imaging. The following images are z-stack maximum intensity projections: Figure 3G, 3K, 3M, 3O, 3Q, Figure 4E-4G, Supplementary Figure 1A, 1B, Figure S2. All images were exported as TIF files. For clarity, cropping and linear exposure adjustments were performed on Adobe Photoshop. Again, settings were matched in negative controls.

Table S1. Primary antibodies, related to Figures 3, 4, 5, S1, S2, S3, S4 and S5.

antibody	**species**	**conc.**	**antigen**	**company**	**reference**	**LOT**	**secondary antibody**
ACE2 (Ab1)	goat	15 µg/ml	Mouse ACE2 extracellular domain, Gln18-Thr740	Invitrogen	PA5-47488	VD2973776	#1, #2

ACE2 (Ab2)	rabbit	1:200	Human ACE2 C-terminal domain, aa 788-805	Abcam	ab15348	GR3333640-4	#3, #5
ACE2 (Ab3)	rabbit	1:200	Human ACE2, extracellular domain, aa 200-300	Abcam	ab108252	GR3338009-3	#3, #5
OMP	goat	1:700	Rodent olfactory marker protein	FUJIFILM Wako	WA3 019-22291	CAG6625	#1 #2
OMP	mouse	1:100	Human olfactory marker protein, aa 1-163	Santa Cruz Biotechnology	sc-365818	E1117	#6, #7
TUJ1	mouse	1:200	Rat brain Tubulin beta 3	Biolegend	801201	B264428	#6, #7
ERMN	rabbit	1:200	Human ERMN	Invitrogen	PA5-58327	R35628	#3, #4, #5
TMPRSS2 (Ab1)	rabbit	1:100	Human TMPRSS2, within aa 1-100	Abcam	ab92323	GR246521-9	#3
TMPRSS2 (Ab2)	rabbit	1:200	Human TMPRSS2, aa 450 to the C-terminus	Abcam	ab109131	GR3248440-2	#3, #4, #5

Table S2. Secondary antibodies, related to related to Figures 3, 4, 5, S1, S2, S3, S4 and S5..

#	**antibody**	**species**	**company**	**reference**
1	anti-goat Alexa 555	donkey	Invitrogen	A21432
2	anti-goat Alexa 488	donkey	Abcam	ab150133
3	anti-rabbit Alexa 555	donkey	Abcam	ab150074
4	anti-rabbit Alexa 488	donkey	Abcam	ab150073
5	anti-rabbit Alexa 488	goat	Life Technologies	A11034
6	anti-mouse Alexa 488	donkey	Abcam	ab150105
7	anti-mouse Cy3	goat	Life Technologies	A10521

Supplemental References

Becht, E., McInnes, L., Healy, J., Dutertre, C.-A., Kwok, I.W.H., Ng, L.G., Ginhoux, F., and Newell, E.W. (2018). Dimensionality reduction for visualizing single-cell data using UMAP. Nature biotechnology.

Benjamini, Y., and Hochberg, Y. (1995). Controlling the false discovery rate: a practical and powerful approach to multiple testing. Journal of the Royal Statistical Society Series B *series B*, 289-300.

Butler, A., Hoffman, P., Smibert, P., Papalexi, E., and Satija, R. (2018). Integrating single-cell transcriptomic data across different conditions, technologies, and species. Nature biotechnology *36*, 411-420.

Dobin, A., Davis, C.A., Schlesinger, F., Drenkow, J., Zaleski, C., Jha, S., Batut, P., Chaisson, M., and Gingeras, T.R. (2013). STAR: ultrafast universal RNA-seq aligner. Bioinformatics *29*, 15-21.

Durante, M.A., Kurtenbach, S., Sargi, Z.B., Harbour, J.W., Choi, R., Kurtenbach, S., Goss, G.M., Matsunami, H., and Goldstein, B.J. (2020). Single-cell analysis of olfactory neurogenesis and differentiation in adult humans. Nature neuroscience *23*, 323-326.

Lake, B.B., Chen, S., Sos, B.C., Fan, J., Kaeser, G.E., Yung, Y.C., Duong, T.E., Gao, D., Chun, J., Kharchenko, P.V.*, et al.* (2018). Integrative single-cell analysis of transcriptional and epigenetic states in the human adult brain. Nature biotechnology *36*, 70-80.

Lawrence, M., Gentleman, R., and Carey, V. (2009). rtracklayer: an R package for interfacing with genome browsers. Bioinformatics *25*, 1841-1842.

Liang, F. (2018). Olfactory receptor neuronal dendrites become mostly intra-sustentacularly enwrapped upon maturity. Journal of Anatomy *232*, 674-685.

Liao, Y., Smyth, G.K., and Shi, W. (2014). featureCounts: an efficient general purpose program for assigning sequence reads to genomic features. Bioinformatics *30*, 923-930.

Love, M.I., Huber, W., and Anders, S. (2014). Moderated estimation of fold change and dispersion for RNA-seq data with DESeq2. Genome biology *15*, 550.

McInnes, L., Healy, J., and Melville, J. (2018). UMAP: Uniform Manifold Approximation and Projection for Dimension Reduction. arXiv.

Satija, R., Farrell, J.A., Gennert, D., Schier, A.F., and Regev, A. (2015). Spatial reconstruction of single-cell gene expression data. Nature biotechnology *33*, 495-502.

Saunders, A., Macosko, E.Z., Wysoker, A., Goldman, M., Krienen, F.M., de Rivera, H., Bien, E., Baum, M., Bortolin, L., Wang, S.*, et al.* (2018). Molecular Diversity and Specializations among the Cells of the Adult Mouse Brain. Cell *174*, 1015-1030.e1016.

Stuart, T., Butler, A., Hoffman, P., Hafemeister, C., Papalexi, E., Mauck, W.M., 3rd, Hao, Y., Stoeckius, M., Smibert, P., and Satija, R. (2019). Comprehensive Integration of Single-Cell Data. Cell *177*, 1888-1902.e1821.

Tang, J., Tang, J., Ling, E.A., Wu, Y., and Liang, F. (2009). Juxtanodin in the rat olfactory epithelium: specific expression in sustentacular cells and preferential subcellular positioning at the apical junctional belt. Neuroscience *161*, 249-258.

Zeisel, A., Hochgerner, H., Lonnerberg, P., Johnsson, A., Memic, F., van der Zwan, J., Haring, M., Braun, E., Borm, L.E., La Manno, G.*, et al.* (2018). Molecular Architecture of the Mouse Nervous System. Cell *174*, 999-1014.e1022.

Zhu, A., Ibrahim, J.G., and Love, M.I. (2019). Heavy-tailed prior distributions for sequence count data: removing the noise and preserving large differences. Bioinformatics *35*, 2084-2092.